Observational constraints on well-posed reconstruction methods and the optimization-Grad-Rubin method

Tahar Amari, J. J. Aly

A&A 522, A52 (2010)
DOI: 10.1051/0004-6361/200913058

Astronomy & Astrophysics

Observational constraints on well-posed reconstruction methods and the optimization-Grad-Rubin method

T. Amari[1,3] and J.-J. Aly[2]

[1] CNRS, Centre de Physique Théorique de l'École Polytechnique, 91128 Palaiseau Cedex, France
e-mail: amari@cpht.polytechnique.fr
[2] AIM, Unité Mixte de Recherche CEA, CNRS, Université Paris VII, UMR 7158, Centre d'Études de Saclay, 91191 Gif-sur-Yvette Cedex, France
[3] Also associate scientist at Observatoire de Paris, LESIA, 5 place Jules Janssen, 92190 Meudon Cedex, France

Received 3 August 2009 / Accepted 3 June 2010

ABSTRACT

Context. Grad-Rubin type methods are interesting candidates for reconstructing the force-free magnetic field of a solar coronal region. As input these methods, however, require the normal component B_n of the field on the whole boundary of the numerical box and the force-free function α on the part of the boundary where $B_n > 0$ (or $B_n < 0$), while observations provide data only on its lower photospheric part. Moreover, they introduce an unpleasing asymmetry between the opposite polarity parts of the boundary, and certainly do not take full advantage of the available data on α.
Aims. We address these issues resulting from observations. We present a possible way to supply the missing information about B_n and α on the non-photospheric sides of the box, and to use more effectively the data provided by the measurements.
Methods. We introduce the optimization-Grad-Rubin method (OGRM), which is in some sense midway between optimization methods and the standard Grad-Rubin methods. It is based on an iterative scheme in which the α used as a boundary condition is imposed to take identical values at both footpoints of any field line and to be as close as possible to the α provided by the measurements on the photosphere. The degree of "closeness" is measured by an "error functional" containing a weight function reflecting the confidence that can be placed on the observational data.
Results. The new method is implemented in our code XTRAPOL, along with some technical improvements. It is thus tested for two specific choices of the weight function by reconstructing a force-free field from data obtained by perturbing in either a random or a non-random way boundary values provided by an exact solution.

Key words. magnetic fields – magnetohydrodynamics (MHD) – methods: data analysis – Sun: corona

1. Introduction

State-of-the-art methods for reconstructing the solar coronal magnetic field have been intensively developed following the arrival of high resolution and low noise vector magnetographs, either on the ground (as THEMIS and SOLIS) or on-board spatial solar missions (such as HINODE and SDO), and before the expected arrival of several new instruments (such as EST or SOLAR-ORBITER). These methods have been elsewhere reviewed (see Aly & Amari 2007; Wiegelmann 2008; Schrijver et al. 2006), and we only reiterate that they can be divided into three main classes: optimization methods (Wiegelmann 2004), which use all the photospheric data and try to determine the field by minimizing a cost function; magnetohydrodynamics relaxation methods (Valori et al. 2005; Mikic & McClymont 1994) and Grad-Rubin methods (Sakurai 1981; Amari et al. 1999; Wheatland 2007). An important difference between optimization and the Grad-Rubin methods is related to the way in which the photospheric data are used. The former uses all the available data but cannot compute from them an exactly force-free field, while the latter uses only a part of the data to set up a well-posed boundary value problem (BVP) for an exactly force-free field.

Amari et al. (2006) presented two different implementations of the well-posed Grad-Rubin boundary value problem (GRBVP), namely XTRAPOL, based on a finite difference approximation, and FEMQ, based on a finite element approximation. As input, both methods require the normal component B_n of the magnetic field on the whole boundary of the computational box, Ω_b, and the values of the force-free function α on that part of the boundary where $B_n > 0$ (or $B_n < 0$). A problem thus appears when one wishes to use these methods to reconstruct the magnetic field of an active region from data furnished by actual measurements. Indeed, the latter provide values of B_n and α only on the lower side S_p of Ω_b, which represents the photospheric part of the region. We then need a method to prescribe the missing boundary values on its lateral and upper sides. In particular, if we compute the coronal field using the values of α in the region S_p^+ of the photosphere where $B_z > 0$, for instance, then we can transport these values along the characteristics (the field lines) into the domain even if they do leave the latter at some point. But for the lines entering the domain from the outside, an additional prescription is needed to relate a value of α to them because they do not connect to S_p^+. A solution may be to impose $\alpha = 0$ on these lines (as was done in Amari et al. 1999), although this would lead to a magnetic field with an energy lower than the energy of the actual field, and errors would then be introduced into the evaluation of the energy budget of pre-eruptive configurations.

Apart from the boundary values of B_n and α, an additional problem is that the field can be reconstructed by solving GRBVP either by using the values of α measured on S_p^+, or those measured on the other polarity, S_p^-, and the two fields obtained in

this way are expected to differ somewhat from each other. The photospheric boundary data are indeed never *compatible* – i.e., no magnetic field in Ω_b matches them – due to the unavoidance of errors in the measurements and the field certainly not being force-free in the dense layer where it is measured, and not even strictly force-free in the corona. Once the field has been reconstructed using the boundary values of α on either S_p^+ or S_p^-, the values of α computed by solving GRBVP most generally do not agree with the measured ones on the other polarity. We then have to determine the best way to perform the reconstruction: imposing α on S_p^+ or imposing α on S_p^-? Or would it not be better to impose that α is given by some average of the values measured at both the footpoints of a magnetic field line?

The aim of this paper is to present a new method, the optimization Grad-Rubin method (OGRM), which provides a possible solution to the questions alluded to above. In OGRM, the boundary values for α are selected by minimizing in some norm the difference between the computed values of α and the measured ones. In some sense, this method is midway between the optimization methods (Wiegelmann 2004) and the Grad-Rubin ones. The plan of the paper is as follows. In Sect. 2, we recall the standard GRBVP and detail the problems one has to face when one wishes to apply it to observational data. The new scheme, OGRM, that we propose for solving them is presented in Sect. 3, and thus tested in Sect. 4 by applying it to the reconstruction of a force-free field from photospheric boundary data obtained by perturbing the boundary values furnished by an analytical model (Low & Lou 1990). Our results are finally summarized in Sect. 5.

After a preliminary version of this paper had been completed, we learned of the work of Wheatland & Regnier (2009), who also discussed the issue of using in a Grad-Rubin scheme the values of α measured along the whole photospheric boundary. We note, however, that the method proposed by these authors to deal with that problem is somewhat different from ours.

2. Grad-Rubin method and the observational constraints problem

2.1. The standard Grad-Rubin method

We define the coronal part above an active region in terms of the bounded computational box $\Omega_b = [x_0, x_1] \times [y_0, y_1] \times [0, z_1]$. The boundary $\partial\Omega_b$ has two parts: the first, $S_p = \partial\Omega_b \cap \{z = 0\}$, lies in the plane $\{z = 0\}$ and represents the photospheric part of the region, while the second, $S_n = \partial\Omega_b \backslash S_p$, is introduced for numerical necessity. We denote as $\hat{\boldsymbol{n}}$ the inner unit normal to $\partial\Omega_b$, such that $\hat{\boldsymbol{n}} = \hat{\boldsymbol{z}}$ on S_p.

The standard Grad-Rubin iterative algorithm for computing the force-free magnetic field $\boldsymbol{B}$ in Ω_b is defined by a couple of hyperbolic and elliptic BVPs given by:

$$\boldsymbol{B}^{(n)}.\nabla\alpha^{(n)} = 0 \quad \text{in} \quad \Omega_b, \tag{1}$$

$$\alpha^{(n)}|_{\partial\Omega_b^+} = \lambda, \tag{2}$$

and

$$\nabla \times \boldsymbol{B}^{(n+1)} = \alpha^{(n)}\boldsymbol{B}^{(n)} \quad \text{in} \quad \Omega_b, \tag{3}$$

$$\nabla \cdot \boldsymbol{B}^{(n+1)} = 0 \quad \text{in} \quad \Omega_b, \tag{4}$$

$$B_n^{(n+1)}|_{\partial\Omega_b} = h_n. \tag{5}$$

The iteration process is initialized by choosing for $\boldsymbol{B}^{(0)}$ the unique solution of

$$\nabla \times \boldsymbol{B}^{(0)} = 0 \quad \text{in} \quad \Omega_b, \tag{6}$$

$$\nabla \cdot \boldsymbol{B}^{(0)} = 0 \quad \text{in} \quad \Omega_b, \tag{7}$$

$$B_n^{(0)}|_{\partial\Omega_b} = h_n, \tag{8}$$

where h_n and λ are the given boundary values for $B_n = \boldsymbol{B} \cdot \hat{\boldsymbol{n}}$ and α, respectively, and $\partial\Omega_b^+ = S_p^+ \cup S_n^+$ is the part of $\partial\Omega_b$ where $h_n > 0$. Alternatively, the value of $\alpha^{(n)}$ may be fixed onto the part $\partial\Omega_b^- = S_p^- \cup S_n^-$ of $\partial\Omega_b$ where $h_n < 0$. There are thus two possible versions of GRBVP, to which we refer hereafter as GR^+ and GR^-, respectively. On the one hand, GR^+ was solved in Amari et al. (2006) by the code XTRAPOL, which uses a vector potential to insure the divergence-less constraint, and on the other hand by the code FEMQ, which dealt with that constraint using a least squares method minimising $\nabla \cdot \boldsymbol{B}$.

Because of the observational constraints, however, the methods used in Amari et al. (2006) are affected by limitations when applied to reconstruct the field of an actual active region. We now examine these limitations.

2.2. Boundary conditions for B_n and α

In the elliptic BVP above, h_n is assumed to be given on the six faces. Observations however only provide h_n on the lower face S_p. This leads us to ask: *How we can use these limited data in the reconstruction method*?

For the hyperbolic part of GR^+, the boundary condition on $\alpha^{(n)}$ is fixed to be on $\partial\Omega_b^+$. The algorithm first computes the characteristics $\boldsymbol{X}^{(n)}(\boldsymbol{r}, s)$ of $\boldsymbol{B}^{(n)}$ passing through $\boldsymbol{r} \in \Omega_b$ as the solution of

$$[\boldsymbol{X}^{(n)}]' = \boldsymbol{B}^{(n)}(\boldsymbol{X}^{(n)}), \tag{9}$$

$$\boldsymbol{X}^{(n)}(\boldsymbol{r}, 0) = \boldsymbol{r}, \tag{10}$$

where the prime symbol represents differentiation with respect to the parameter s that runs along the characteristic. The value of $\alpha^{(n)}$ at $\boldsymbol{r}$ is thus set equal to

$$\alpha^{(n)}(\boldsymbol{r}) = \lambda[\boldsymbol{X}_+^{(n)}(\boldsymbol{r})], \tag{11}$$

where we use the notation $\boldsymbol{X}_\pm(\boldsymbol{r}) = \{\boldsymbol{X}(\boldsymbol{r}; s)\} \cap \partial\Omega_b^\pm$ for the footpoints of the characteristic $\boldsymbol{X}$ on the positive and negative polarity parts of the boundary, respectively.

On S_p^+, λ can be evaluated from the measured magnetic field $\boldsymbol{h}$ by using the relation

$$\lambda = \frac{1}{h_z}\left(\frac{\partial h_y}{\partial x} - \frac{\partial h_x}{\partial y}\right), \tag{12}$$

and Eq. (11) can be immediately used when $\boldsymbol{X}_+^{(n)}(\boldsymbol{r}) \in S_p^+$. But a problem arises when $\boldsymbol{X}_+^{(n)}(\boldsymbol{r}) \in S_n^+$, as we have no observed value λ at that point. We are thus faced with the following question: *Which value should be attributed to* $\alpha^{(n)}(\boldsymbol{r})$ *in that situation?* In Amari et al. (2006), this problem did not occur because the two computational methods were tested only in cases where λ is given on the whole $\partial\Omega_b$. A simple possibility, adopted in Amari et al. (1999), consists of imposing $\alpha^{(n)} = 0$ at those locations, but this leads to zero electric current along the associated characteristics, and then to a magnetic field with an energy lower than the energy of the actual field.

2.3. Photospheric measurement errors and non force-free boundary

We consider a characteristic $\boldsymbol{X}(\boldsymbol{r}, s)$ of the field computed by GR^+, and assume that it connects S_p^+ to S_p^- and then carries a value of α equal to the value of λ at its footpoint on S_p^+. Regardless of the methods used to answer the two questions above, this value is most generally expected to differ somewhat

from the value of λ given at its computed footpoint on $S_{\rm p}^-$ by the measurements. This is due to the various reasons already enumerated in the introduction: observational errors in the measurements of $\boldsymbol{h}$, likely importance of the nonmagnetic forces in the layer where the measurements are effected, and, to a lesser extent, in the corona itself. In other words, the observational data (h_z, λ) on $S_{\rm p}$ are most generally *inconsistent with each other*. They are not even expected to satisfy the necessary condition of compatibility (Aly 1989)

$$\int_{S_{\rm p}} \Theta(\pm\lambda - \tau) h_z \, {\rm d}s = 0, \tag{13}$$

where Θ is the standard Heaviside function and $\tau \geq 0$ an arbitrary number (this constraint is exact only if we consider $\Omega_{\rm b}$ to be the whole half-space $\{z > 0\}$, although it has to still hold true for some range of sufficiently large values of τ in the general situation where the larger values of λ are reached in the central part of $S_{\rm p}$). The discrepancy between the computed and measured values of α on $S_{\rm p}^-$ may be estimated by the number

$$\Delta^+ = \int_{S_{\rm p}^-} |\alpha - \lambda|^2 g|h_z| \, {\rm d}s = \int_{S_{\rm p}^-} |\lambda^+ - \lambda|^2 g|h_z| \, {\rm d}s, \tag{14}$$

where $\lambda^+(\boldsymbol{r}) = \lambda[\boldsymbol{X}_+(\boldsymbol{r})]$ and $g|h_z| > 0$ is some weight function introduced to take into account the degree of confidence one may have in the accuracy of the data. A proper choice may actually be $g = 1$, which places more weight on the regions of strong fields where the measurements of λ are more reliable. The reconstruction may clearly be considered to be of some value only if

$$\Delta^+ \ll \int_{S_{\rm p}^-} |\lambda|^2 g|h_z| \, {\rm d}s. \tag{15}$$

The same line of arguments of course, applies (up to a change in signs) if we consider GR$^-$ instead of GR$^+$.

If we apply both methods GR$^\pm$ to the same data, we can a posteriori compare the number $\Delta^\pm$ and select the reconstruction that provides the smallest error. Continuing this line of thought a little further, one may also ask whether *it would be possible to diminish some quadratic distance between the measured values λ and the computed ones on the whole $S_{\rm p}$ by imposing α in the formulation of GRBVP to take on $S_{\rm p}^+$ a value $\lambda_1 \neq \lambda$, but as close as possible to λ*?

We note that this question relates to the idea of *preprocessing the data*, which has been used in relation to the optimization methods of reconstruction (Wiegelmann et al. 2006). Preprocessing consists of modifying as little as possible (in some sense) the actual data $\boldsymbol{h}$ to make them satisfy some necessary global constraints of compatibility (Aly 1989). A simple preprocessing of the values of λ may consist here of requiring λ_1 to satisfy the set of constraints presented in Eq. (13). This operation, however, appears to be difficult to implement even if we restrict ourselves to a small number of values of τ, and we proceed in a somewhat simpler way in the next section.

3. The optimization Grad-Rubin method (OGRM)

We now present our revisited Grad-Rubin type algorithm (OGRM), which gives a possible solution to the issues discussed in the previous section.

3.1. Boundary condition for B_n

In all cases, we assume that on the horizontal rectangle $S_{\rm p}$, the function $h_{\rm n}$ is given by the observations and takes the value $h_{\rm n} = h_z$.

For the "numerical" boundary $S_{\rm n}$, a possible (and most common) choice would be to insist that

$$h_{\rm n} = 0, \tag{16}$$

which of course is allowed only if the magnetic flux $\int_{S_{\rm p}} h_z \, {\rm d}s = 0$ (if this is not the case, our reconstruction scheme could be applied only after preprocessing the h_z-data to ensure that the total flux vanishes). With the boundary condition Eq. (16) being enforced, the magnetic lines of the force-free field $\boldsymbol{B}$ do not go across $S_{\rm n}$ and magnetic connections between the domain to which reconstruction is applied and its environment are thus not allowed. This may be an unwanted feature as this domain is most generally non magnetically isolated, either because the part $S_{\rm p}$ of the photosphere over which data are available does not cover all the active region to which it belongs, or because it is connected by bundles of magnetic lines to other regions. Moreover, this assumption makes the computed field certainly more compressed than the actual one, which may lead to an overestimate of the magnetic energy.

Another possibility would be to assume that

$$h_{\rm n} = B_{\pi {\rm n}} \quad \text{on} \quad S_{\rm n}, \tag{17}$$

with the potential field $\boldsymbol{B}_\pi(x, y, z) = \nabla V_\pi(x, y, z)$ being computed by solving the BVP

$$\nabla^2 V_\pi = 0 \qquad \text{in } \{z > 0\}, \tag{18}$$

$$\frac{\partial V_\pi}{\partial z} = \begin{cases} h_z & \text{on } S_{\rm p}, \\ 0 & \text{on } \{z = 0\} \backslash S_{\rm p}, \end{cases} \tag{19}$$

$$rV_\pi = {}_{r\to\infty} O(1) \tag{20}$$

set in the whole half-space. The solution can be written in the explicit form

$$V_\pi(\boldsymbol{r}) = -\frac{1}{2\pi} \int_{S_{\rm p}} \frac{h_z(\boldsymbol{r}')}{|\boldsymbol{r} - \boldsymbol{r}'|} \, {\rm d}s', \tag{21}$$

and is valid even when the photospheric flux is non-zero (in the latter case, $\boldsymbol{B}_\pi$ has open lines extending to infinity). In contrast to the first choice: (i) this one leads to a non-zero $h_{\rm n}$ on $S_{\rm n}$, and allows the computation of a magnetic field and its associated current, which may enter or leave $\Omega_{\rm b}$ across $S_{\rm n}$; (ii) the computed field is minimally confined as $\boldsymbol{B}_\pi$ expands into the whole half-space, while being generated by a h_z vanishing outside $S_{\rm p}$.

Instead of one of the two conditions above, we choose the boundary condition

$$h_{\rm n} = B_{\pi {\rm n}} \quad \text{on} \quad S_{\rm n}, \tag{22}$$

with the potential field $\boldsymbol{B}_\pi(x, y, z) = \nabla V_\pi(x, y, z)$ now being computed by solving the mixed (Neumann-Dirichlet) BVP

$$\nabla^2 V_\pi = 0 \qquad \text{in } \Omega_{\rm b}, \tag{23}$$

$$\frac{\partial V_\pi}{\partial z} = h_z \qquad \text{on } S_{\rm p}, \tag{24}$$

$$V_\pi = 0 \qquad \text{on } S_{\rm n}. \tag{25}$$

As the previous one, this choice of $h_{\rm n}$ allows the field and the current to cross $S_{\rm n}$. This may be considered here to be a direct consequence of the last boundary condition, Eq. (25), which

causes $\boldsymbol{B}_\pi$ to be normal to S_n. From the point of view of the confinement of $\boldsymbol{B}$ in Ω_b, this property may be expected to make the computed field (whose lines will actually be no longer strictly normal to S_n) somewhere between those computed with the two first choices of h_n, and it may be argued that the action exerted on the field by the magnetic environment of the region is to some extent more accurately taken into account than it is with the two first choices of h_n. We add finally that previous test cases have shown that the present choice of h_n on S_n provides optimal results for the reconstructed field when combined with a method for fixing the boundary condition on α, which allows current to flow through S_n. It is quite possible, however, that the improvement is due mainly to the latter factor.

3.2. Computation of the vector potential

In our code XTRAPOL, the condition $\nabla \cdot \boldsymbol{B}^{(n)} = 0$ is imposed by introducing a vector potential $\boldsymbol{A}^{(n)}$ and ensuring that the iterated field $\boldsymbol{B}^{(n)} = \nabla \times \boldsymbol{A}^{(n)}$. $\boldsymbol{A}^{(n)}$ satisfies the gauge and boundary conditions

$$\nabla \cdot \boldsymbol{A}^{(n)} = 0 \qquad \text{in } \Omega_\mathrm{b}, \tag{26}$$

$$\boldsymbol{A}^{(n)}_\mathrm{t} = \boldsymbol{A}_{\pi\mathrm{t}} \qquad \text{on } \partial\Omega_\mathrm{b}, \tag{27}$$

where $\boldsymbol{A}_\pi$ is a specific vector potential of the potential field $\boldsymbol{B}_\pi$ such that $\nabla \cdot \boldsymbol{A}_\pi = 0$, and $\boldsymbol{X}_\mathrm{t}$ denotes the component of $\boldsymbol{X}$ tangential to the boundary. In Amari et al. (2006), $\boldsymbol{A}_\pi$ was uniquely fixed by the boundary condition $\nabla_\mathrm{t} \cdot \boldsymbol{A}_{\pi\mathrm{t}} = 0$ on $\partial\Omega_\mathrm{b}$. Its computation from h_n thus required us to solve a 2D Poisson equation on that entire surface, considered as a single 2D domain, with the continuity of $\boldsymbol{A}_\mathrm{t}$ at the edges being ensured by solving an asymmetric linear system. This method proved to be efficient for the test cases (reconstruction of an analytically known force-free field), but we found that the convergence of the algorithm was sensitive to data smoothness when considering true active regions. We therefore modify the computation of $\boldsymbol{A}_{\pi\mathrm{t}}$ to develop a much more robust method.

In our new scheme, $\boldsymbol{A}_\pi$ is constructed as follows. It must satisfy the gauge condition $A_{\pi z} = 0$, and thus be of the general form (DeVore 2000)

$$\boldsymbol{A}_\pi(x,y,z) = \boldsymbol{A}_0(x,y) + \int_0^z \boldsymbol{B}_\pi(x,y,z')\mathrm{d}z' \times \hat{\boldsymbol{z}}. \tag{28}$$

The lower boundary value $\boldsymbol{A}_0(x,y) = \boldsymbol{A}_\pi(x,y,0)$ must satisfy

$$\hat{\boldsymbol{z}} \cdot (\nabla_\perp \times \boldsymbol{A}_0)(x,y) = h_z(x,y,0), \tag{29}$$

(where $\nabla_\perp = \hat{\boldsymbol{x}}\partial_x + \hat{\boldsymbol{y}}\partial_y$) and is defined only up to the addition of the gradient of an arbitrary function $f(x,y)$. To fix this remaining gauge arbitrariness, we also impose

$$\nabla_\perp \cdot \boldsymbol{A}_0 = 0, \tag{30}$$

which implies, along with the equation $\nabla \times \boldsymbol{B}_\pi = 0$, the required condition

$$\nabla \cdot \boldsymbol{A}_\pi = 0 \qquad \text{in } \Omega_\mathrm{b}. \tag{31}$$

There does clearly exist a function $\chi_\pi(x,y,z)$ such that

$$\boldsymbol{A}_\pi = \nabla\chi_\pi \times \hat{\boldsymbol{z}}, \tag{32}$$

where χ_π satisfies the relation

$$\chi_\pi(x,y,z) = \chi(x,y) + \int_0^z V_\pi(x,y,z')\,\mathrm{d}z', \tag{33}$$

and $\chi(x,y) = \chi_\pi(x,y,0)$, which can be readily applied to solve the equation

$$-\nabla^2_\perp \chi_\pi(x,y,z) = B_z(x,y,z) \qquad \text{in } \Omega_\mathrm{b}. \tag{34}$$

To determine effectively $\boldsymbol{A}_\pi$ on $\partial\Omega_\mathrm{b}$, we proceed as follows. We first compute the function $\chi_\pi(x,y,0)$ in S_p by solving the 2D Poisson equation given by Eq. (34) (with $z = 0$) with the boundary condition

$$\chi_\pi(x,y,0) = 0 \quad \text{on } \partial S_\mathrm{p}. \tag{35}$$

We thus obtain $\boldsymbol{A}_\pi(x,y,0) = \nabla\chi_\pi(x,y,0) \times \hat{\boldsymbol{z}}$. We next use Eq. (28) and the values of $\boldsymbol{A}_\pi$ on ∂S_p to derive $\boldsymbol{A}_\pi$ on the vertical part of $\partial\Omega_\mathrm{b}$. We finally obtain $\boldsymbol{A}_\pi(x,y,z_1)$ by solving Eq. (34) (now with $z = z_1$) along with the Neumann boundary condition $\partial_n\chi_\pi(x,y,z_1) = (\hat{\boldsymbol{n}} \times \hat{\boldsymbol{z}}) \cdot \boldsymbol{A}_\pi$ on the boundary of the upper face (where $\boldsymbol{A}_\pi$ is known from the previous step). We note that $\boldsymbol{A}_\pi$ is tangential to $\partial\Omega_\mathrm{b}$: as a mere consequence of the gauge condition $A_{\pi z} = 0$ on the lower and upper horizontal faces, and as a consequence of Eqs. (33), (35), and (25) on the vertical ones.

3.3. Boundary condition for α

To start with, we define the *error functional*

$$O[\boldsymbol{B},\mu;g] = \int_{S_\mathrm{p}} |\mu - \lambda|^2 g |B_z|\,\mathrm{d}s, \tag{36}$$

which is used to measure the closeness between the boundary values imposed on α and the measured values λ. In that expression, $\boldsymbol{B}$ is an arbitrary magnetic field in Ω_b (with $B_\mathrm{n} = h_\mathrm{n}$ on $\partial\Omega_\mathrm{b}$), μ is an arbitrary function defined on $\partial\Omega_\mathrm{b}$ taking the same value at both footpoints of an arbitrary line of $\boldsymbol{B}$, i.e.,

$$\mu(\boldsymbol{r}) = \mu(\boldsymbol{X}_-(\boldsymbol{r})) \qquad \text{for } \boldsymbol{r} \in \partial\Omega^+_\mathrm{b}, \tag{37}$$

and $g|B_z| \geq 0$ is some fixed weight function (as in Eq. (14), the factor $|h_z|$ has been singled out for convenience). This weight function is supposed to represent the confidence that can be placed on the values of λ computed from the three components of the measured field, and thus must be fixed on the basis of instrumental considerations (not discussed here). Quite naturally, we extend g to the whole $\partial\Omega_\mathrm{b}$ by setting $g = 0$ on S_n, where no observational data are available.

By flux conservation along a thin flux tube, we have $(B_\mathrm{n}\,\mathrm{d}s)(\boldsymbol{r}) = -(B_\mathrm{n}\,\mathrm{d}s)(\boldsymbol{X}_+(\boldsymbol{r}))$ for $\boldsymbol{r} \in \partial\Omega^-_\mathrm{b}$, and can rewrite the functional O in the form

$$O[\boldsymbol{B},\mu;g] = \int_{\partial\Omega^+_\mathrm{b}} \left[|\mu - \lambda|^2 g + |\mu - \Lambda|^2 G\right] |B_\mathrm{n}|\,\mathrm{d}s, \tag{38}$$

where we have set $(G,\Lambda)(\boldsymbol{r}) = (g,\lambda)(\boldsymbol{X}_-(\boldsymbol{r}))$ for $\boldsymbol{r} \in S^+_\mathrm{p}$, and λ has been extended in an arbitrary way to S^+_n (where $g = 0$). By developing the squares in the integrand in the right-hand side of Eq. (38) and by rearranging the terms, we derive the alternative formula

$$\begin{aligned} O[\boldsymbol{B},\mu;g] &= \int_{S^+} \left[(g+G)\left(\mu - \underline{\mu}\right)^2 + \frac{gG}{g+G}(\lambda - \Lambda)^2\right] |B_z|\,\mathrm{d}s \\ &\geq \int_{S^+} \frac{gG}{g+G}(\lambda - \Lambda)^2 |B_z|\,\mathrm{d}s, \end{aligned} \tag{39}$$

where we have introduced the function $\underline{\mu}$ defined on $\partial\Omega^+_\mathrm{b}$ by

$$\underline{\mu} = \frac{\lambda g + \Lambda G}{g+G}\cdot \tag{40}$$

It is then quite clear that, for fixed magnetic field $\boldsymbol{B}$ and boundary data λ, $O[\boldsymbol{B}, \mu; g]$ is minimized by the function $\underline{\mu}$, with its minimum value being given by

$$\underline{O}[\boldsymbol{B}; g] = O[\boldsymbol{B}, \underline{\mu}; g] = \int_{\partial\Omega_{\rm b}^+} \frac{gG}{g+G}(\lambda - \Lambda)^2 |B_{\rm n}| \, {\rm d}s. \tag{41}$$

The latter is to be compared with the value

$$O[\boldsymbol{B}, \mu_0; g] = \int_{\partial\Omega_{\rm b}^+} G(\lambda - \Lambda)^2 |B_{\rm n}| \, {\rm d}s, \tag{42}$$

assumed by O when we take for μ the function μ_0 satisfying $\mu_0 = \lambda$ on $S_{\rm p}^+$. We note that a standard variational argument applied to Eq. (38) would have given immediately $\underline{\mu}$ as an extremizer, but some more work would then have been needed to demonstrate that $O[\boldsymbol{B}, \underline{\mu}; g]$ is a minimum.

To obtain a possible solution to the third question addressed in the previous section, we now introduce the *optimization-Grad-Rubin problem (OGRP)*, for which we attempt to *determine a couple of terms* $(\boldsymbol{B}, \alpha)$ *in* $\Omega_{\rm b}$ *satisfying the equations and boundary conditions of the standard Grad-Rubin problem, but with a boundary condition for* α *on* $\partial\Omega_{\rm b}^+$ *that is self-consistently determined in such a way that the functional* $O[\boldsymbol{B}, \alpha; g]$ *takes its lowest possible value.*

Equation (40) suggests trying to solve OGRP by using a simple modification of the standard Grad-Rubin iterative scheme into which we could substitute the boundary condition given by Eq. (2) by

$$\alpha^{(n)} = \frac{\lambda g + \Lambda^{(n)} G^{(n)}}{g + G^{(n)}} \quad \text{on} \quad \partial\Omega_{\rm b}^+, \tag{43}$$

where $(\Lambda^{(n)}, G^{(n)})(\boldsymbol{r}) = (\lambda, g)(\boldsymbol{X}_+^{(n)}(\boldsymbol{r}))$ and we recall that $\boldsymbol{X}^{(n)}(\boldsymbol{r}, s)$ denotes the characteristics associated with $\boldsymbol{B}^{(n)}$. We note that the boundary condition changes at each iteration step, and that OGRM is based on a coprocessing of the boundary data on λ, in contradistinction to an a priori preprocessing such as that used in Wiegelmann et al. (2006). The jump from GR$^{\pm}$ to OGRM clearly does not entail many complications. In the modified scheme, we have to extend the line through each point $\boldsymbol{r}$ in $\Omega_{\rm b}$ in both directions (towards $\partial\Omega_{\rm b}^+$ and $\partial\Omega_{\rm b}^-$), while we had to do this in only one direction (towards $\partial\Omega_{\rm b}^+$) when dealing with the standard scheme.

The condition illustrated by Eq. (43) may be detailed as follows. Firstly when both footpoints of $\boldsymbol{X}^{(n)}(\boldsymbol{r}, s)$ are located on $S_{\rm p}$, this characteristic receives a value of $\alpha^{(n)}$, which is some average between the values of λ at $\boldsymbol{X}_+^{(n)}$ and $\boldsymbol{X}_-^{(n)}$, respectively. If we choose for instance $g = 1$ on $S_{\rm p}$, we find that

$$\alpha^{(n)} = \frac{\lambda + \Lambda^{(n)}}{2}, \tag{44}$$

which is merely the arithmetic mean of the values of λ at its footpoints. A similar value appears in Inhester & Wiegelmann (2006), but with a somewhat different justification. Secondly when $\boldsymbol{X}^{(n)}(\boldsymbol{r}, s)$ connects $S_{\rm n}^+$ (where $g = 0$) to $S_{\rm p}^-$, it receives the value $\alpha^{(n)} = \Lambda^{(n)}$, i.e.,

$$\alpha^{(n)}(\boldsymbol{r}) = \lambda[\boldsymbol{X}_-^{(n)}(\boldsymbol{r})]. \tag{45}$$

OGRM thus also answers the second question set in Sect. 2.2. We note that it provides in general a nonzero value for $\alpha^{(n)}$ on the characteristics entering $\Omega_{\rm b}$ through $S_{\rm n}^+$.

We conclude this section by pointing out the main difference between our method for taking into account the values of λ on the whole $S_{\rm p}$ and the method proposed by Wheatland & Regnier (2009). We reach our final force-free field after a single series of iterations, but Wheatland & Regnier (2009) require a double series of iterations to obtain theirs. They indeed compute a sequence of force-free fields by alternatively solving either a GR$^+$ or a GR$^-$. More precisely, they start with the computation of a force-free field $\boldsymbol{B}_1$ by GR$^+$, i.e., by using the values of λ on $S_{\rm p}^+$. A field $\boldsymbol{B}_2$ is thus computed by GR$^-$, with the boundary values of α on $S_{\rm p}^-$ being taken to be equal to some average between the observational values λ and the values of α_1 computed at the previous step. The process is thus reiterated until convergence of the sequence $\{\boldsymbol{B}_k\}$ is obtained.

4. Test cases

4.1. General method

We check the effectiveness of OGRM by computing a series of test cases performed with a numerical resolution of 64^3. Since OGRM depends on the choice of a function g, we denote it as OGRM(g) hereafter because two different choices of g are under simultaneous consideration. We note that GR$^{\pm}$ may be considered to be OGRM($g^{\pm}$), respectively, where $g^{\pm} = 1$ on $S_{\rm p}^{\pm}$, and $g^{\pm} = 0$ on $S_{\rm p}^{\mp}$.

As in Amari et al. (2006), we use for our tests a particular analytical force-free field that belongs to the well-known class derived in Low & Lou (1990, referred to hereafter as LowLou solution). This solution is defined by the parameters $FFF1 := (n = 1, m = 1, L = .3, \Phi = \pi/4)$. As OGRM may differ significantly from GR$^{\pm}$ only when the boundary data are not compatible, we construct an "observed" function λ by perturbing the exact boundary value $\alpha_{\rm exact}$ taken on $S_{\rm p}$ by the analytic α-function. We use two types of perturbations – nonrandom and random, respectively –, each one being supposed to represent some errors in the photospheric measurements. For each data set obtained in this way: (i) we reconstruct the field using four methods: GR$^+$, GR$^-$, OGRM($g = 1$), and OGRM($g = \mid B_{\rm n} \mid^{-1}$); (ii) we analyse their convergence by considering the behaviours of the quantity

$$\eta^{(n)} = \frac{||\boldsymbol{B}^{(n+1)} - \boldsymbol{B}^{(n)}||_{L^2}}{||\boldsymbol{B}^{(n)}||_{L^2}} \tag{46}$$

and the norm $||\boldsymbol{B}^{(n)}||_{L^2}$, where

$$||\boldsymbol{X}||_{L^2} = \left(\int_{\Omega_{\rm b}} |\boldsymbol{X}|^2 \, {\rm d}v \right)^{1/2}; \tag{47}$$

(iii) we compare the values taken by the error functional $O[g]$ in which we take successively $g = 1$ and $g = |B_{\rm n}|^{-1}$. Our choices of g are somewhat arbitrary, being made here just for convenience, and we do not claim that they are the relevant ones for applications to actual data (rather, the choice of g for a set of actual data should be made after a thorough analysis of the observational errors, ...). We note that it makes sense to evaluate $O[g]$ even for a solution computed with OGRM(g'), with $g' \neq g$. In $O[g]$, the weight g is determined by the quality of the observations, and once it has been fixed, $O[g]$ may be used to evaluate the quality of a solution obtained from the data $(h_{\rm n}, \lambda)$ by any means – e.g., by using OGRM[g']. Of course, what we wish to check is that the optimal result – i.e., the lowest value of $O[g]$ – is obtained for OGRM(g). Finally, we also point out that the reconstruction of a perturbed state even with GR$^+$ and GR$^-$, constitutes a test of the continuity of the solutions with respect to changes in the boundary conditions (i.e., one of the conditions for having a well-posed problem).

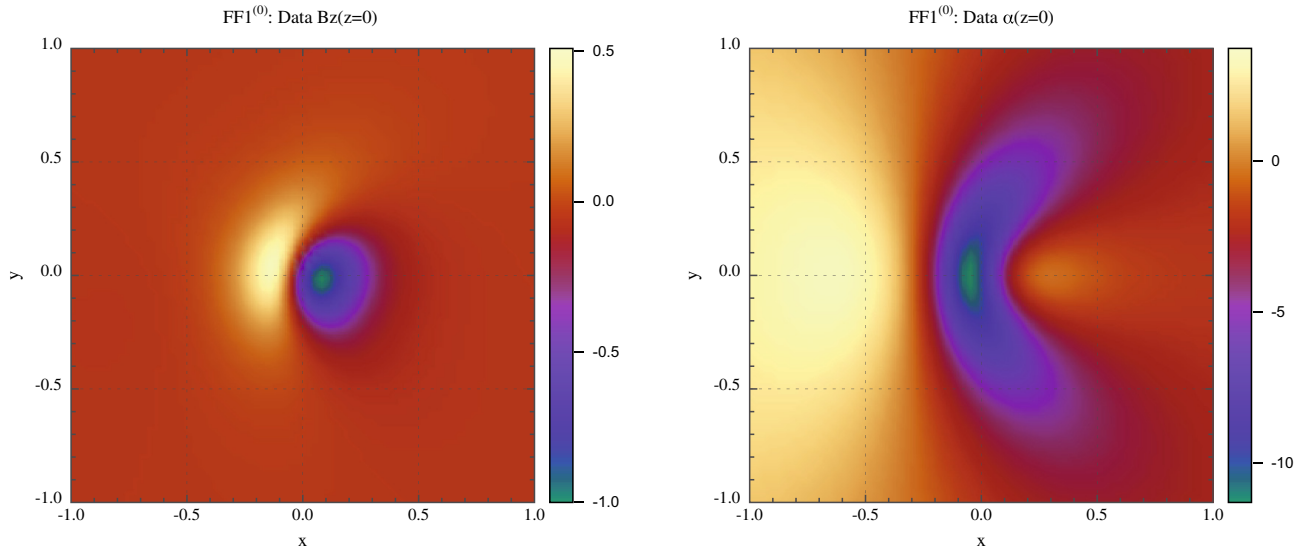

Fig. 1. Distributions on S_p of B_z and $\lambda = \alpha_{\rm Exact}$ for the reference case FFF1$^{(0)}$.

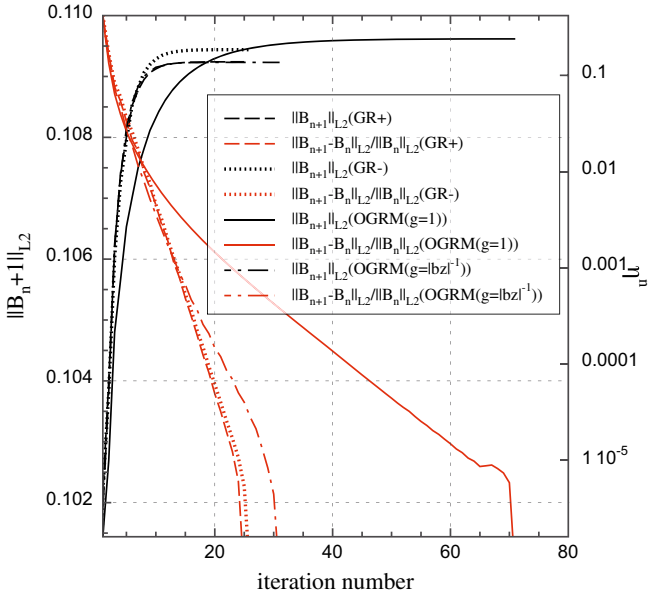

Fig. 2. Convergence properties of the four methods GR$^+$, GR$^-$, OGRM($g = 1$), and OGRM($g = |B_n|^{-1}$), in the reference case FFF1$^{(0)}$. The convergence rate is fast and the norm of the solution reaches its asymptotical value in about 15 iterations, apart from the case of OGRM($g = 1$), which converges at a slightly lower rate requiring about 30 iterations.

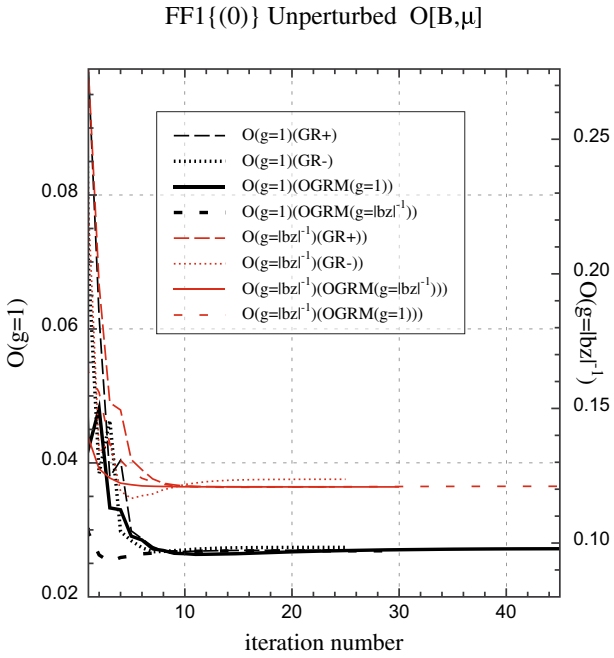

Fig. 3. Error functionals $O(g = 1)$ and $O(g = |B_n|^{-1})$, for the four methods GR$^+$, GR$^-$, OGRM($g = 1$), and OGRM($g = |B_n|^{-1}$), applied to the reference case FFF1$^{(0)}$. The four methods lead to almost the same small value for these errors, with a slight advantage for OGRM($g = 1$) and OGRM($g = |B_n|^{-1}$).

4.2. Reference case

As a preliminary test, we first consider the case (referred to as FFF1$^{(0)}$) defined by the boundary condition $\lambda = \alpha_{\rm Exact}$ on S_p, for which we should ideally expect the four methods to lead to the exact force-free LowLou solution. However, as noticed in Amari et al. (2006), some errors caused by the discretisation and interpolation on the computational grid cannot be completely eliminated, and we already have a situation where small departures from compatibility are present. Figure 1 shows the distributions of B_z and λ on S_p for this reference case.

As can be seen in Fig. 2, and as expected, the four methods converge rapidly for this unperturbed case, although at a somewhat lower rate for OGRM($g = 1$). Figure 3 also shows that they behave almost identically, reaching in particular the same value of O.

4.3. Nonrandom perturbation

We next consider a boundary function λ obtained from $\alpha_{\rm Exact}$ by applying a specific nonrandom perturbation. The new λ, which defines the case FFF1$^{(t_+,t_-)}$, is given by

$$\lambda^{(t_+,t_-)}(x,y) = (1+t_+)\alpha_{\rm Exact}(x,y) \quad \text{on} \quad S_p^+, \tag{48}$$

$$\lambda^{(t_+,t_-)}(x,y) = (1-t_-)\alpha_{\rm Exact}(x,y) \quad \text{on} \quad S_p^-, \tag{49}$$

where t_+ and t_- are real numbers in $[0, 1[$.

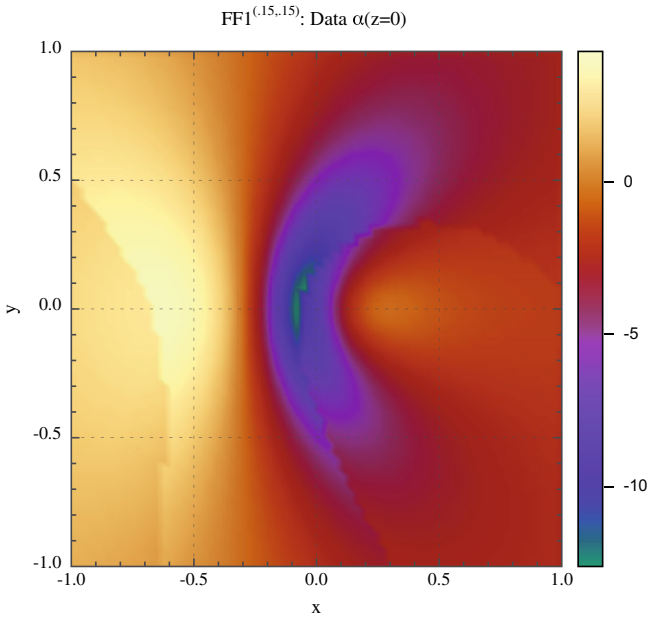

Fig. 4. Distribution on S_p of $\lambda^{(0.15,0.15)}$ obtained by perturbing $\alpha_{\rm Exact}$ in a nonrandom way.

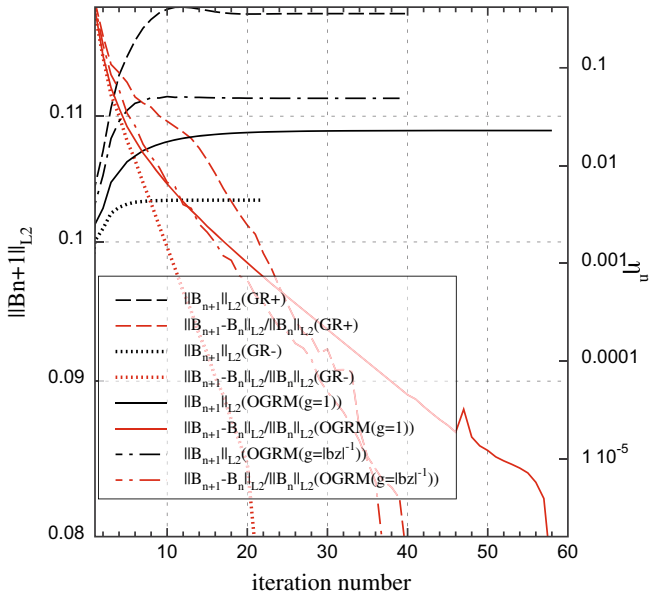

Fig. 5. Convergence properties of the four methods GR$^+$, GR$^-$, OGRM($g=1$), and OGRM($g=|B_n|^{-1}$), in the non randomly perturbed case case FFF1$^{(.15,.15)}$. The convergence rate is fast, even if lower for OGRM($g=1$).

We first consider the symmetric case FFF1$^{(0.15,0.15)}$, whose corresponding $\lambda^{(0.15,0.15)}$ on S_p is shown in Fig. 4. As can be seen in Fig. 5, the four methods lead once more to a low value of the convergence parameter $\eta^{(n)}$, with the smallest value being obtained for OGRM($g=1$).

It is also clear in Fig. 6, which shows the two error functionals $\mathcal{O}(g=1)$ and $\mathcal{O}(g=|B_n|^{-1})$, that the two methods OGRM($g=1$) and OGRM($g=|B_n|^{-1}$) lead to smaller errors than those obtained with GR$^+$ and GR$^-$ (although with a lower difference for the latter).

For the case FFF1$^{(0.1,0.4)}$ corresponding to the asymmetric choice of parameters $t_+ = 0.1$ for S_p^+ and $t_- = 0.4$ on S_p^- in Eq. (49) defining our non randomly perturbed boundary

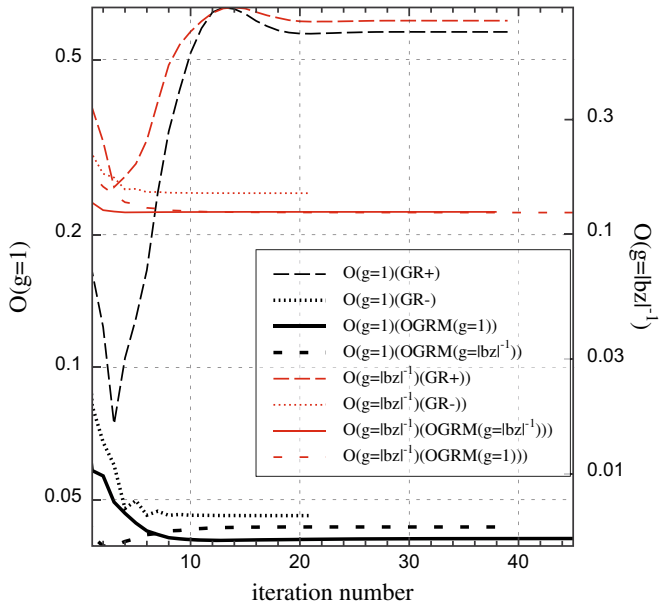

Fig. 6. Error functionals $\mathcal{O}(g=1)$ and $\mathcal{O}(g=|B_n|^{-1})$ for the four methods GR$^+$, GR$^-$, OGRM($g=1$), and OGRM($g=|B_n|^{-1}$), applied to the non randomly perturbed case FFF1$^{(.15,.15)}$. The optimal results are obtained with OGRM($g=1$), OGRM($g=|B_n|^{-1}$), and OGRM($g=|B_n|^{-1}$), which is even slightly better.

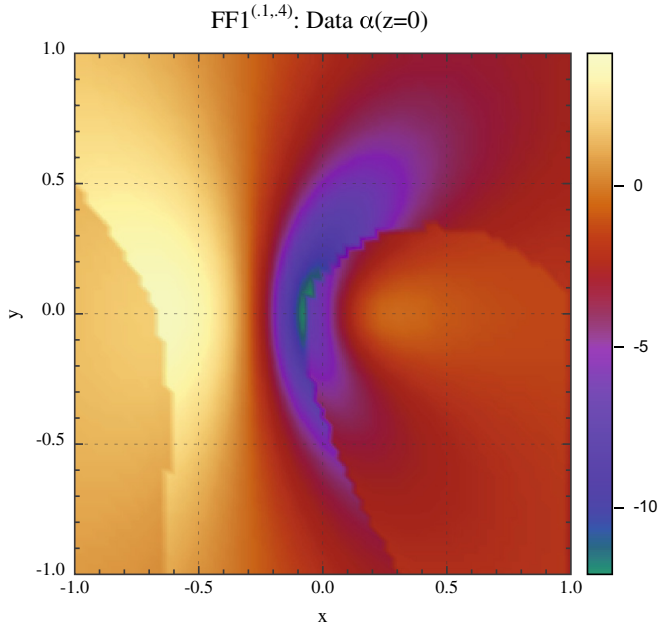

Fig. 7. Distribution of $\lambda^{(.1,.4)}$ obtained from $\alpha_{\rm Exact}$ by a nonrandom perturbation defined by the parameters $t_+ = 0.1$ in S_p^+ and $t_- = 0.4$ on S_p^-.

condition, the corresponding $\lambda^{(0.1,0.4)}$ is shown in Fig. 7. The four methods converge at about the same fast rate, as shown in Fig. 8, but the difference in behaviour is accentuated (see Fig. 9). Indeed, while the two weighted methods are clearly better than the original GR$^+$ and GR$^-$, OGRM($g=|B_n|^{-1}$) infers lower error values than OGRM($g=1$). This shows the effect of the weight in our method.

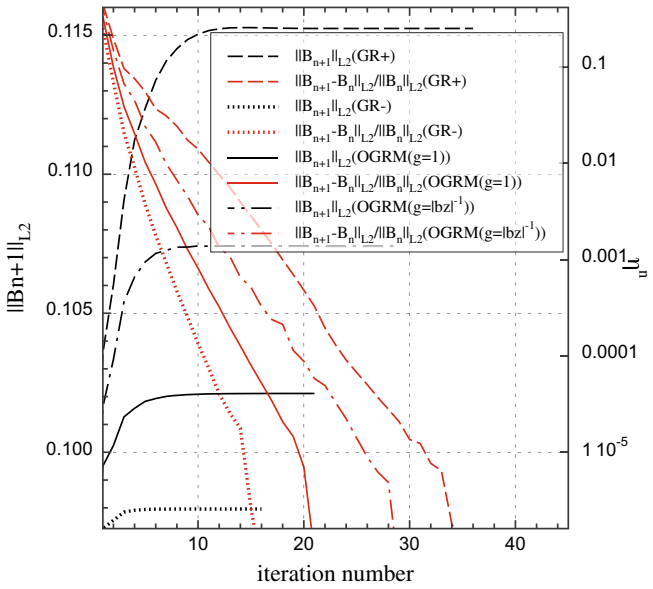

Fig. 8. Convergence properties of the four methods GR$^+$, GR$^-$, OGRM($g = 1$), and OGRM($g = |B_n|^{-1}$), applied to the non randomly perturbed case case FFF1$^{(.1,.4)}$.

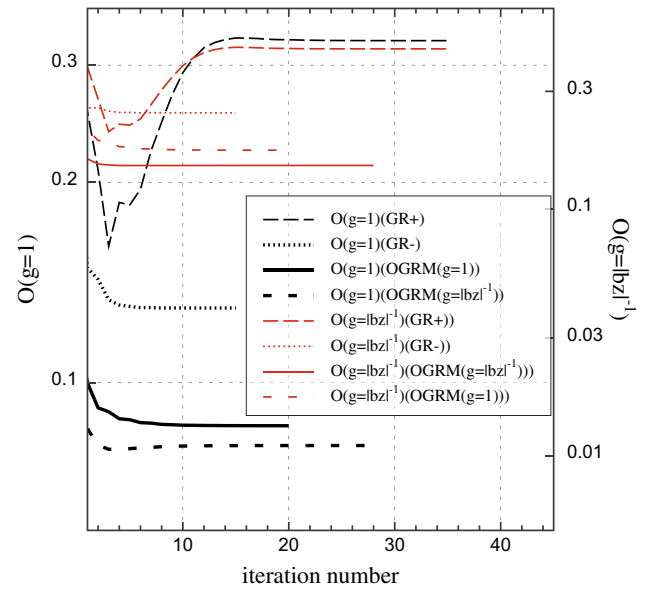

Fig. 9. Error functionals $\mathcal{O}(g = 1)$ and $\mathcal{O}(g = |B_n|^{-1})$ for the four methods GR$^+$, GR$^-$, OGRM($g = 1$), and OGRM($g = |B_n|^{-1}$), in the non randomly perturbed case FFF1$^{(.1,.4)}$. The best results are obtained with OGRM($g = |B_n|^{-1}$).

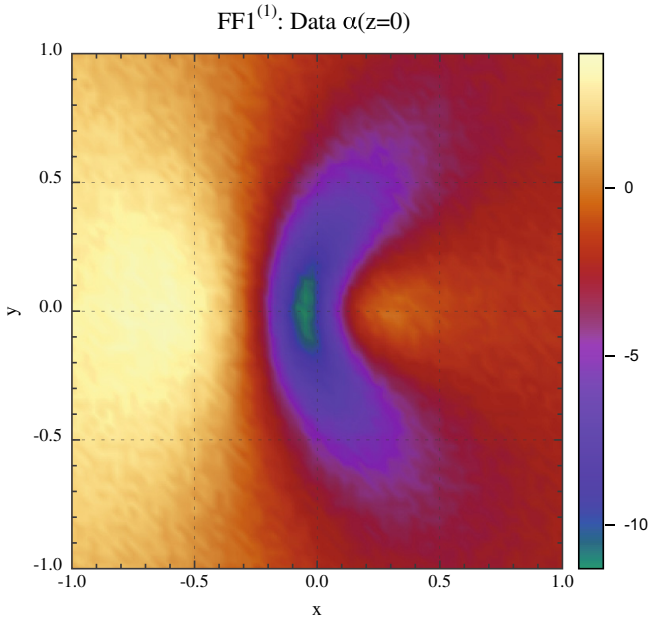

Fig. 10. Distribution of $\lambda^{(1)}$ obtained from $\alpha_{\rm Exact}$ by a random perturbation defined by Eq. (51) with $\delta = 1$.

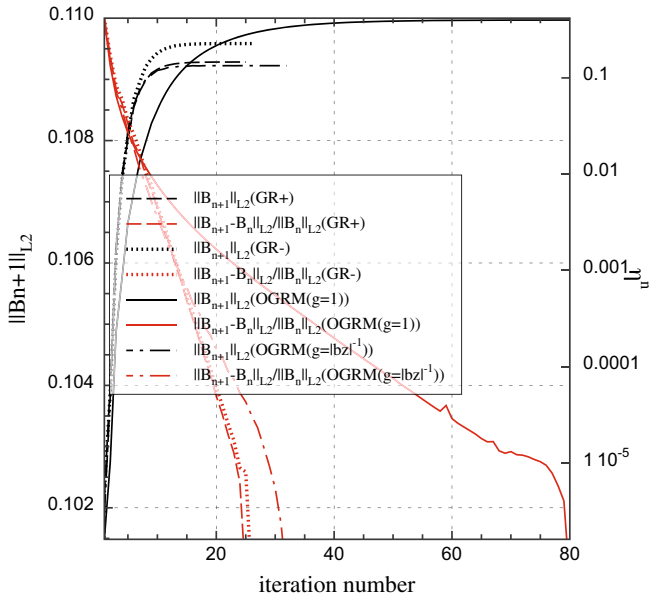

Fig. 11. Convergence properties of the four methods GR$^+$, GR$^-$, OGRM($g = 1$), and OGRM($g = |B_n|^{-1}$), applied to the randomly perturbed case case FFF1$^{(1)}$.

4.4. Random perturbation

We finally apply to the reference boundary function $\alpha_{\rm Exact}$ a random perturbation that produces a λ of the form

$$\lambda^{(\delta)}(x, y) = \alpha_{\rm Exact}(x, y) + \delta f(x, y) \quad \text{on} \quad S_{\rm p}, \tag{50}$$

$$f(x, y) = 2\, Random(x, y) - 1, \tag{51}$$

where *Random* is a random function taking its values in $[0, 1]$, and δ is a positive coefficient controlling the magnitude of the perturbation. The perturbation can thus take both signs on S, with no special correlation between its values on $S_{\rm p}^+$ or $S_{\rm p}^-$. We refer to the corresponding randomly perturbed state as FFF1$^{(\delta)}$, and consider two particular values of δ.

As can be seen in Fig. 10, the random perturbation is relatively moderate in the FFF1$^{(1)}$ case. Moreover, one can already see that the four methods converge rapidly, with a lower rate for OGRM($g = 1$), while OGRM($g = |B_n|^{-1}$) converges almost as rapidly as the original GR$^+$ and GR$^-$. By inspecting the error functional diagnostics shown in Fig. 11, we see that the four methods perform almost identically well, with a slight superiority for the two weighted methods.

We finally consider the randomly perturbed case FFF1$^{(10)}$ corresponding to the strong perturbation seen in Fig. 13. The four methods converge to different values (see Fig. 14), with the smallest values being found for GR$^+$ and GR$^-$. The values reached by OGRM($g = 1$) and OGRM($g = |B_n|^{-1}$), although larger, can be considered as accurate for such a strong

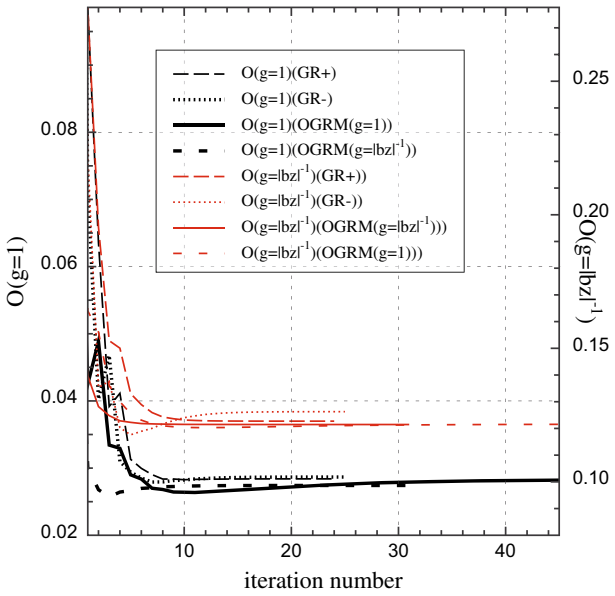

Fig. 12. Error functionals $\mathcal{O}(g=1)$ and $\mathcal{O}(g=|B_n|^{-1})$ for the four methods GR$^+$, GR$^-$, OGRM($g=1$), and OGRM($g=|B_n|^{-1}$), applied to the randomly perturbed case FFF1$^{(1)}$. The best results are obtained with OGRM($g=|B_n|^{-1}$).

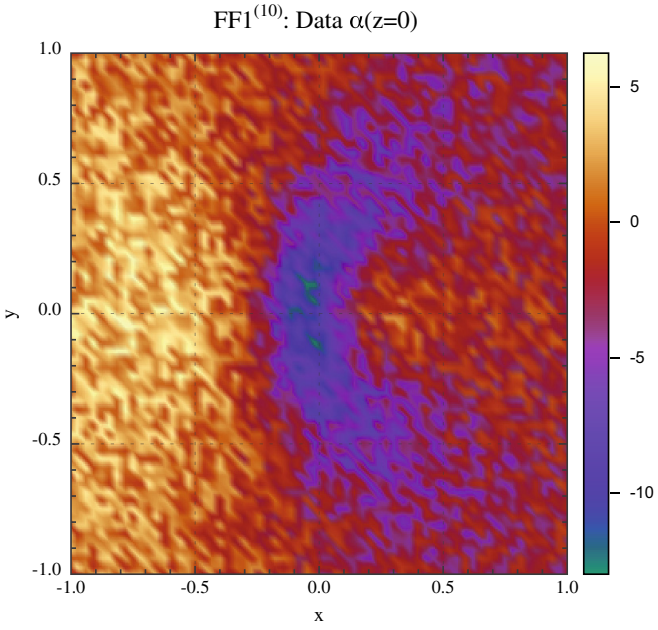

Fig. 13. Distribution on S_p of $\mathcal{A}^{(10)}$ obtained from $\alpha_{\rm Exact}$ by a random perturbation defined by Eq. (51) with $\delta = 10$.

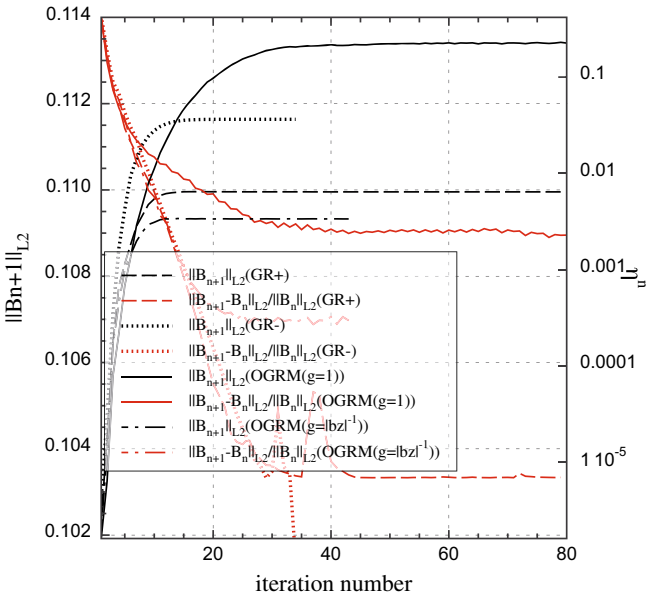

Fig. 14. Convergence properties of the four methods GR$^+$, GR$^-$, OGRM($g=1$), and OGRM($g=|B_n|^{-1}$), applied to the randomly perturbed case FFF1$^{(10)}$.

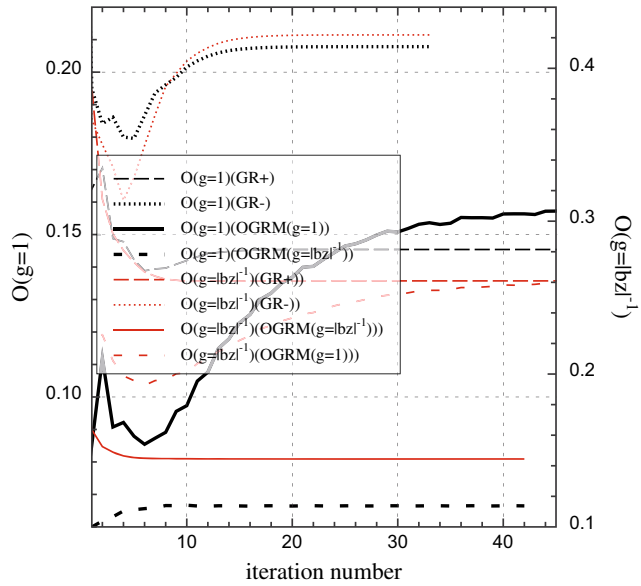

Fig. 15. Error functionals $\mathcal{O}(g=1)$ and $\mathcal{O}(g=|B_n|^{-1})$ for the four methods GR$^+$, GR$^-$, OGRM($g=1$), and OGRM($g=|B_n|^{-1}$), applied to the randomly perturbed case FFF1$^{(10)}$. The best results are obtained with OGRM($g=|B_n|^{-1}$).

perturbation. The error functional diagnostics gathered in Fig. 15 clearly show that OGRM($g=|B_n|^{-1}$) provides the lowest error. This clearly shows that in the case of a strong perturbation the choice of weight $g=|B_n|^{-1}$) leads to a lower error (in the sense explained above) than the choice corresponding to $g=1$.

5. Conclusion

We have addressed some issues that arise when one wishes to reconstruct the field of a coronal active region using one of our previously presented Grad-Rubin type schemes (Amari et al. 2006) and observationally acquired data. A first issue is related to the computations always being performed in a finite box: this introduces an artificial "numerical boundary" over which the observations which are obtained only at the photospheric level, do not furnish the required boundary conditions for both the normal component of the field and the force-free function α. The problem is thus to account in some way for this lack of data. The second issue arises from the values of B_n and α measured at the photospheric level never being "compatible" because of the errors in the observations and their treatment (e.g., in the disambiguation of the transverse field), and because the actual field is far from being force-free in the photospheric layers, and not even exactly force-free in the corona. A disagreement is found when the field is reconstructed by one of our earlier methods – either GR$^+$ or GR$^-$: the values of α computed in the polarity where this quantity is not imposed do not match those measured in this

polarity. Here the problem one is naturally led to face is what is the most accurate determination of the boundary condition on α to be used in the hyperbolic part of GRBVP.

We have proposed to answer the two questions above by introducing a new method, OGRM(g), where g is some weight function. In OGRM(g), the value of B_n on the "numerical part" S_n of the boundary is constrained to be equal to that of the potential field computed as follows: its normal component is constrained to be equal to the measured one on the photospheric part S_p of the boundary, while its tangential component vanishes on S_n. This choice is in some sense intermediate between two other more common choices, the one in which the potential field is fully confined inside the numerical box, and the one in which this field is allowed to fully expand into the whole half-space. As the latter, it allows the field and the current to go across the numerical boundary, which is most generally a desirable feature because the region whose field is reconstructed is not magnetically isolated from its environment. As for the boundary condition imposed on α, it is selected in OGRM(g) by trying to minimize an error functional (depending on g) measuring the difference between the computed boundary values of α and the measured ones. This selection cannot be made a priori, as the error functional depends on the field that has to be computed. But we have shown mathematically that it is possible to make that choice in a step by step way, by setting up a new Grad-Rubin type algorithm. In OGRM, at each iteration α is assumed to be equal to some weighted average of the values measured at both the footpoints of a line (or the value taken at its photospheric footpoint when one footpoint lies on the numerical boundary). This method is in some sense midway between the optimization methods that use all the available data but cannot compute from them an exact force-free field, and the Grad-Rubin ones that use only half of the data (B_n being fixed on $\partial\Omega_b$, and α on either $\partial\Omega_b^+$ or $\partial\Omega_b^-$) to compute an exactly force-free field. Compared to GR$^{\pm}$ developed in Amari et al. (2006), OGRM(g) does not require either far more iterations or a new internal iteration loop. Moreover, it does not distinguish between the solutions obtained by imposing α on the positive and negative polarity, respectively. In that sense OGRM(g) is symmetric by construction, and is based on a unique BVP. As we have already pointed out, it is not the first time that the values of α measured over the whole photospheric boundary are used as an input for a Grad-Rubin scheme. Proposals have already been made by Inhester & Wiegelmann (2006) and by Wheatland & Regnier (2009), which differ from ours in one way or another.

We have applied OGRM(g) to a series of test cases in which the "photospheric" values of α are obtained by perturbing the α_{Exact} provided by a LowLou force-free field. We have used two types of perturbations, random and nonrandom, and used for both the reconstruction and the error functional, two different weight functions: (i) $g = 1$, which corresponds to substituting into the error functional an actual weight $g|B_n| = |B_n|$ that provides greater importance to the high field regions, and attributes to each characteristic a value of α equal to the arithmetic average of the values measured at its footpoints when both lie in the photosphere; (ii) $g = |B_n^{-1}|$, which corresponds to an actual weight function $g|B_n| = 1$ in the error functional and thus appears to place all the regions on the same footing. These somewhat arbitrary choices proved to be adequate for testing the convergence and efficiency of OGRM(g). But for the reconstruction of the field of an actual active region, a thorough analysis of the observational conditions in which the data have been obtained is of course necessary to determine g. The latter depends on quantities such as the norm of the transverse field and the magnitude of the polarisation errors (as in the "stress and relax" method of Roumeliotis 1996), and are set to zero where data are of particularly poor quality, ... The new scheme OGRM(g) has been found to have convergence properties comparable to those of the old ones, GR$^{\pm}$. It is just a bit slower (requiring more iterations), which should be related to the boundary condition on α changing at each step. The best results (in the sense of minimisation of error functional) have been obtained with OGRM($g = |B_n^{-1}|$), which proved to be the most robust method corresponding to the lowest discrepancies between the measured values of α and the computed ones on the photospheric boundary.

We note that we do not claim that OGRM solves the issue related to the non force-free character of the magnetic field in the layer where it is measured: OGRM just provides a possible way of using as well as possible the data obtained by the currently available instruments. The "non force-free" issue is common to all the force-free reconstruction methods, and its solution is likely to require the construction of a more general class of models in which both the corona and a subphotospheric layer are treated in similar ways.

Acknowledgements. We are grateful to the referee, B. Inhester, for his constructive comments, which led to an improved version of the paper. T.A. thanks A. Canou for discussion. We would also like to thank the Centre National d'Études Spatiales (CNES) for support.

References

Aly, J.-J. 1989, Sol. Phys., 120, 19
Aly, J.-J., & Amari, T. 2007, Geophys. Astrophys. Fluid Dyna., 101, 249
Amari, T., Boulmezaoud, T. Z., & Mikic, Z. 1999, A&A, 350, 1051
Amari, T., Boulmezaoud, T. Z., & Aly, J.-J. 2006, A&A, 446, 691
DeVore, C. R. 2000, ApJ, 539, 944
Inhester, B., & Wiegelmann, T. 2006, Sol. Phys., 235, 201
Low, B. C., & Lou, Y. Q. 1990, ApJ, 352, 343
Mikic, Z., & McClymont, A. N. 1994, in Solar Active Region Evolution: Comparing Models with Observations, ed. K. S. Balasubramaniam, & G. W. Simon, ASP Conf. Ser., 68, 225
Roumeliotis, G. 1996, ApJ, 473, 1095
Sakurai, T. 1981, Sol. Phys., 69, 343
Schrijver, C. J., Derosa, M. L., Metcalf, T. R., et al. 2006, Sol. Phys., 235, 161
Valori, G., Kliem, B., & Keppens, R. 2005, A&A, 433, 335
Wheatland, M. 2007, Sol. Phys., 245, 251
Wheatland, M. S., & Régnier, S. 2009, ApJ, 700, L88
Wiegelmann, T. 2004, Sol. Phys., 219, 87
Wiegelmann, T. 2008, J. Geophys. Res. (Space Phys.), 113, 3
Wiegelmann, T., Inhester, B., & Sakurai, T. 2006, Sol. Phys., 233, 215